


## ORIGINAL ARTICLE

# Ferroptosis resistance determines high susceptibility of murine *A/J* strain to iron-induced renal carcinogenesis

Zhen Cheng<sup>1</sup> | Shinya Akatsuka<sup>1</sup> | Guang Hua Li<sup>1</sup> | Kiyoshi Mori<sup>2,3,4</sup> | Takashi Takahashi<sup>5</sup>  | Shinya Toyokuni<sup>1,6</sup> 

<sup>1</sup>Department of Pathology and Biological Responses, Nagoya University Graduate School of Medicine, Nagoya, Japan

<sup>2</sup>Graduate School of Public Health, Shizuoka Graduate University of Public Health, Shizuoka, Japan

<sup>3</sup>Department of Molecular and Clinical Pharmacology, School of Pharmaceutical Sciences, University of Shizuoka, Shizuoka, Japan

<sup>4</sup>Department of Nephrology and Kidney Research, Shizuoka General Hospital, Shizuoka, Japan

<sup>5</sup>Aichi Cancer Center Research Institute, Nagoya, Japan

<sup>6</sup>Center for Low-temperature Plasma Sciences, Nagoya University, Nagoya, Japan

## Correspondence

Shinya Toyokuni, Department of Pathology and Biological Responses, Nagoya University Graduate School of Medicine, 65 Tsurumai-cho, Showa-ku, Nagoya, 466-8550, Japan. Email: toyokuni@med.nagoya-u.ac.jp

## Funding information

JST CREST, Grant/Award Number: JPMJCR19H4; JSPS, Grant/Award Number: JP19H05462 and JP20H05502; Princess Takamatsu Cancer Research

## Abstract

Cancer susceptibility is a critical factor in the understanding of carcinogenesis. Intraperitoneal (i.p.) injection of an iron chelate, ferric nitrilotriacetate (Fe-NTA), produces hydroxyl radicals via Fenton reaction to induce ferroptosis in renal proximal tubules. Rats or mice subjected to repeated i.p. injections of Fe-NTA develop renal cell carcinoma (RCC). To elucidate the molecular mechanisms that cause susceptibility to renal carcinogenesis, we first established an inter-strain difference in the susceptibility to Fe-NTA-induced renal carcinogenesis in mice. Based on a previous observation of a low incidence of RCC with this model in *C57BL/6J* strain mice, we investigated *A/J* strain mice here, which demonstrated significantly higher susceptibility to Fe-NTA-induced renal carcinogenesis. Homozygous deletion of the *Cdkn2a/2b* tumor suppressor locus was detected for the first time in *A/J* strain mice. Focusing on ferroptosis and iron metabolism, we explored the mechanisms involved that lead to the difference in RCC development. We compared the protective responses in the kidney of *A/J* and *C57BL/6J* strains after Fe-NTA treatment. After 3-week Fe-NTA treatment, *A/J* mice maintained higher levels of expression of glutathione peroxidase 4 and xCT (SLC7A11), leading to a lower level of lipid peroxidation. Simultaneously, *A/J* mice had decreased expression of transferrin receptor and increased expression of ferritin to greater degrees than *C57BL/6* mice. After a single Fe-NTA injection, higher levels of oxidative cell damage and cytosolic catalytic Fe(II) were observed in *C57BL/6J* mice, accompanied by a greater increase in lipocalin-2. Lipocalin-2 deficiency significantly decreased oxidative renal damage. Our results suggest that a genetic trait favoring ferroptosis resistance contributes to high susceptibility to Fe-NTA-induced RCC in *A/J* strain.

## KEYWORDS

animal models, ferroptosis, iron, lipocalins, renal cell carcinoma

This is an open access article under the terms of the Creative Commons Attribution-NonCommercial-NoDerivs License, which permits use and distribution in any medium, provided the original work is properly cited, the use is non-commercial and no modifications or adaptations are made.

© 2021 The Authors. *Cancer Science* published by John Wiley & Sons Australia, Ltd on behalf of Japanese Cancer Association.

## 1 | INTRODUCTION

Iron is essential for human life.<sup>1</sup> The iron balance in our body is maintained through both systemic and cellular regulatory mechanisms.<sup>2-4</sup> Iron is not only associated with multiple physiological processes but is also involved in various pathological conditions, including inflammation, anemia and cancer. Iron-mediated cellular toxicity has been recognized as one of the key factors in renal injury and carcinogenesis.<sup>5-7</sup> Except for some hereditary renal cell carcinomas (RCC), such as those associated with germline mutations of *VHL*, *MET*, or *FLCN*,<sup>8</sup> most human RCC originate from somatic mutations. Therefore, it is important to establish animal models to replicate the process of human renal carcinogenesis.<sup>9</sup>

Intraperitoneal (i.p.) injection of ferric nitrilotriacetate (Fe-NTA), a form of chelated iron, produces reactive oxygen species (ROS), including hydroxyl radicals, via Fenton reaction in the renal proximal tubules in mice and rats.<sup>10</sup> In the first half of the 1980s, our research group established that repeated i.p. administration of Fe-NTA induces a very high incidence of RCC in rats (approximately 90%).<sup>6,11</sup> For mice, we also succeeded in obtaining RCC at approximately 60% incidence with *A/J* strain in 1987.<sup>12</sup> However, in the recent experiments using *C57BL/6J* mice, the incidence of RCC was low (<10%).<sup>13</sup> Therefore, it is necessary to clarify the mechanisms responsible for the inter-strain difference in susceptibility to Fe-NTA-induced renal carcinogenesis. In the first mouse carcinogenesis experiment with *A/J* strain mice, mice were observed for only 60 weeks, whereas our recent experiment with the *C57BL/6J* strain of mice followed all the mice for 120 weeks. In the present study, we performed the renal carcinogenesis experiment with *A/J* mice, with all mice followed until the point of death to establish the inter-strain difference. Genomic DNA exposed to ROS may develop copy number aberrations and somatic mutations, which potentially are the basis for carcinogenesis.<sup>14</sup> ROS may affect specific chromosomal loci to provoke carcinogenesis.<sup>15</sup> The genome of Fe-NTA-induced rat RCC carries prominent chromosomal aberrations, which frequently include homozygous deletion of the *Cdkn2a/2b* tumor suppressor and amplification of the *Met* oncogene.<sup>16</sup> However, RCC induced in *C57BL/6J* wild-type mice and *C57BL/6J* background *Mutyh*-knockout mice exhibited less chromosomal aberrations in comparison to rat RCC.<sup>13</sup> Here, we applied array-based comparative genomic hybridization (aCGH) to

compare the chromosomal aberrations in the obtained RCC between *A/J* mice and *C57BL/6J* mice or rats.

We also analyzed acute/subacute responses to the Fe-NTA-induced renal damage in *A/J* and *C57BL/6J* mice to identify the underlying mechanism for the difference in susceptibility. We hypothesized that ferroptosis and iron metabolism are involved in the susceptibility to Fe-NTA-induced renal carcinogenesis. The catalytic Fe(II) in cytosol, called labile iron pool (LIP), can be highly reactive and produces various ROS.<sup>17,18</sup> Ferroptosis is a type of regulated cell death, defined as catalytic Fe(II)-dependent regulated necrosis accompanying lipid peroxidation.<sup>19</sup> Ferroptosis is regulated by cellular glutathione and glutathione peroxidase 4 (GPX4)<sup>20</sup> as well as by iron regulatory/metabolizing proteins. Transferrin receptor 1 (TfR1), a membrane protein binding to the transferrin complex to uptake iron to cytoplasm,<sup>21</sup> not only controls the cellular iron level but can be a ferroptosis marker.<sup>22</sup> Lipocalin 2 (LCN2), also called neutrophil gelatinase-associated lipocalin (NGAL), is a small secreted protein that binds to iron via siderophores to promote cellular iron uptake or induce apoptosis to contribute to renal injury.<sup>23</sup> The early phase analyses suggested that inherent ferroptosis resistance of the renal tubular cells in *A/J* mice determines the difference in carcinogenesis from *C57BL/6J* mice.

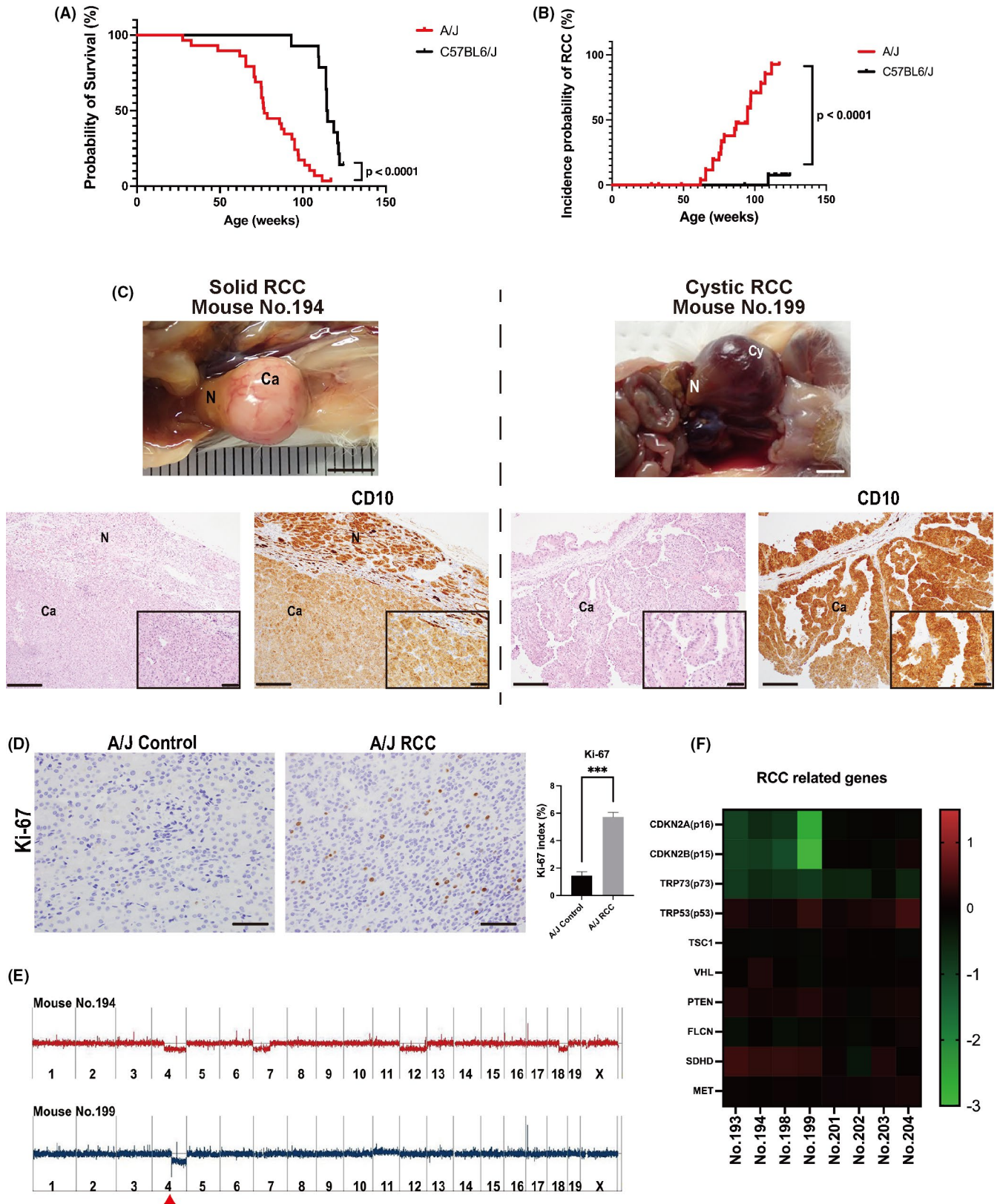
## 2 | MATERIALS AND METHODS

### 2.1 | Protocols for ferric nitrilotriacetate induced renal carcinogenesis in mice

Ferric nitrate enneahydrate was obtained from Wako, and nitrilotriacetic acid disodium salt was obtained from TCI (Tokyo, Japan); they were dissolved in deionized water to make 300 and 600 mM solutions, respectively. The solution of ferric nitrate enneahydrate and nitrilotriacetic acid disodium was mixed immediately before use to make Fe-NTA solution, with a ratio of 1:2 (v/v); the pH was adjusted to 7.4 with sodium carbonate (Wako). Finally, the Fe-NTA solution was diluted 10 times with deionized water. All the chemicals used were of analytical grade.

From 4 weeks of age, 58 male wild-type *A/J* mice were maintained under a standard diet at the laboratory animal facility of Nagoya University Graduate School of Medicine. All the mice were injected i.p. with Fe-NTA, with a dose of 5 mg iron/kg five times a week for

**FIGURE 1** High incidence of ferric nitrilotriacetate (Fe-NTA)-induced renal cell carcinomas (RCC) and *Cdkn2a/2b* homozygous deletion in *A/J* mice. (A) Kaplan-Meier survival curves in *A/J* and *C57BL/6J* strains (determined using log-rank [Mantel-Cox] test). (B) The incidence probability of Fe-NTA induced RCC in *A/J* and *C57BL/6J* strains (determined using log-rank [Mantel-Cox] test). (C) Macroscopic images of solid RCC (bar = 5 mm) and cystic RCC (bar = 10 mm) from *A/J* mice. Microscopic images of solid RCC and cystic RCC from *A/J* mice with H&E staining and CD10 immunohistochemistry (IHC; bar = 200  $\mu$ m; bar = 50  $\mu$ m in the insets). Ca, carcinoma; Cy, cyst; N, normal tissue. (D) Immunohistochemical staining of Ki-67 (bar = 50  $\mu$ m). Ki-67 index, ratio of Ki-67 positive cells to total cells (N = 3 for control; N = 7 for RCC; \*\*\**P* < .001). (E) Array-based comparative genomic hybridization (CGH) analysis of two representative cases of RCC in *A/J* mice (refer to Figure S2 for other six cases). The number at the bottom of the image corresponds to each murine chromosome. Red arrowhead, homozygous deletion of *Cdkn2a/2b*. (F) Heat map of array-based CGH analysis of eight cases of RCC in *A/J* mice regarding the orthologous genes that represent germline mutation in human hereditary RCCs. Data on *C57BL/6J* strain in (A, B) was obtained from our previous report<sup>13</sup> and reevaluated



the first 2 weeks, and injected with a dose of 7 mg iron/kg five times a week during the next 10 weeks. The mice that were found dying were killed. The fresh kidney tissues were either fixed in 10% PBS for H&E staining/immunohistochemistry or frozen at -80°C for other analyses.

## 2.2 | Protocols for ferric nitrilotriacetate-induced acute and subacute renal injury in mice

Regarding the acute renal injury experiments, 7 male *A/J* wild-type mice, 7 male *C57BL/6J* wild-type mice and three *C57BL/6J Lcn2 (-/-)*

mice were used. *A/J wild-type* and *C57BL/6J wild-type* mice were purchased from SLC. *Lcn2 (-/-)* mice with a *C57BL/6* background were generated as described previously.<sup>24</sup> At 4-weeks old, all mice were injected i.p. with 5 mg iron/kg Fe-NTA; mice were killed 3 hours later. For the subacute renal injury experiments, 3 male *A/J wild-type* mice and 3 male *C57BL/6J wild-type* mice were used. The Fe-NTA i.p. injection was as follows: the first two days at 3 mg iron/kg and the following days at 5 mg iron/kg. The mice were killed 24 hours after

the final injection of Fe-NTA. The animal experimental committee of Nagoya University Graduate School of Medicine approved all the animal experiments described.

### 2.3 | Immunoblot analysis

Renal tissue samples were homogenized in RIPA buffer with protease inhibitor. The tissue lysates were centrifuged at 21,600 x g for 15 minutes at 4°C. The supernatant was collected and stored at -80°C. A Protein Assay Bicinchoninate Kit (Nacalai Tesque) was used to quantify the protein. According to the standard protocol, proteins were separated with SDS-PAGE and transferred onto PVDF membranes, which were incubated in blocking buffer (5% defatted milk) at 4°C overnight. They were then hybridized with the primary antibody for 2 hours and then HRP-conjugated secondary antibody for 30 minutes at room temperature (RT), followed by reaction with the Chemi-Lumi One Ultra Super Kit (Nacalai Tesque). Finally, the bands were visualized with LuminoGraph I (ATTO, Tokyo, Japan) and quantified with ImageJ software (<https://imagej.nih.gov/ij/>).

TABLE 1 Summary of obtained tumors in Fe-NTA-treated mice

Mouse strain	<i>A/J</i>	<i>C57BL/6J</i> <sup>a</sup>
Total mice	29	14
Lung adenocarcinoma	2	0
Lymphoma	0	6
Renal cell carcinoma	18	1
RCC incidence	18/29 (62.07%)	1/14 (7.14%)

Fe-NTA, ferric nitrilotriacetate; RCC, renal cell carcinoma.

<sup>a</sup>Data from our previous report.<sup>13</sup>

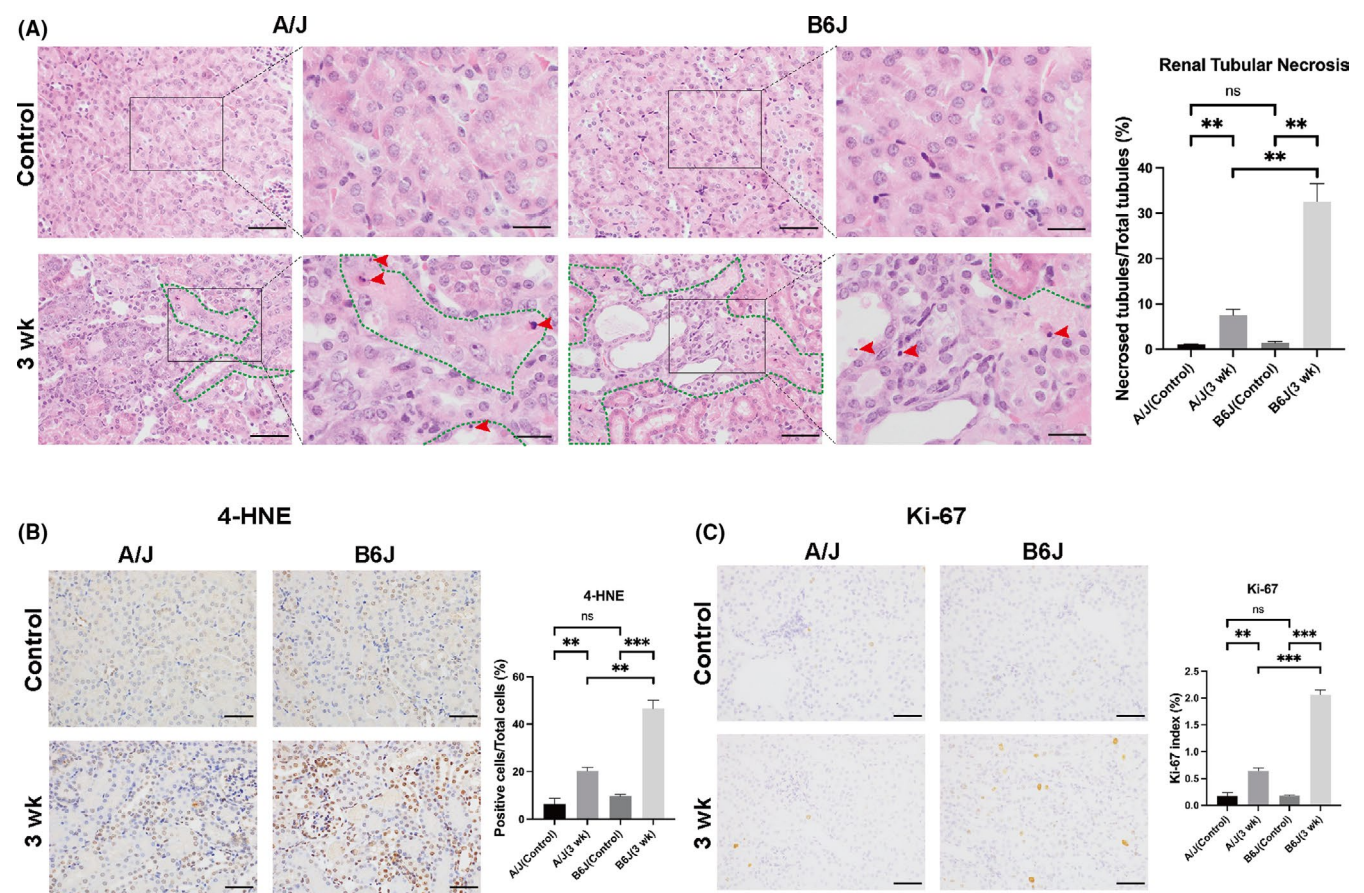


FIGURE 2 Ferroptosis is repressed in *A/J* mice after repeated intraperitoneal (i.p.) administration of ferric nitrilotriacetate (Fe-NTA) for 3 weeks. (A) Lower level of renal proximal tubular necrosis in *A/J* mice with H&E staining in comparison to *C57BL/6J* mice. Green dotted lines delineate the region of renal tubular necrosis. Red arrowheads, pyknosis (bar = 50  $\mu$ m or 20  $\mu$ m in each right magnified panel; N = 3). (B) Lower level of 4-hydroxy-2-nonenal (4-HNE) in *A/J* mice with immunohistochemistry (IHC) analysis in comparison to *C57BL/6J* mice (bar = 50  $\mu$ m; N = 3). (C) Lower level of Ki-67 in *A/J* mice with IHC analysis in comparison to *C57BL/6J* mice (bar = 50  $\mu$ m; N = 3; mean  $\pm$  SEM; \*P < .05, \*\*P < .01, \*\*\*P < .001; ns, not significant). Refer to text for details

## 2.4 | Immunohistochemistry and renal tubular damage analysis

LCN2 and Ki-67 immunohistochemical staining were performed manually. Antigen retrieval was performed in 10 mM pH 6.0 sodium citrate buffer, at 100°C for 5 minutes. Samples were blocked by Serum Free Reagent (x0909, DAKO) for 15 minutes and incubated with primary antibody for 1.5 hours at RT, followed by HRP-conjugated second antibody for 30 minutes at RT. Finally, the slides were visualized with a DAB kit (K3468, DAKO). Other immunostaining was performed by BOND MAX/III (Leica) with BOND Polymer Refine Detection (ds9800; Leica). ImageJ was used to quantify the

integrated density. For the renal tubular damage analysis in H&E-stained specimens, the proximal tubules with nuclear pyknosis and membrane disruption were regarded as damaged. We randomly selected the microscopic cortical areas from 3 mice of each group to calculate the ratio of damaged renal tubules to total renal tubules.

## 2.5 | Antibodies

The following primary antibodies were used for immunoblot analysis and immunohistochemistry: mouse monoclonal anti-transferrin receptor antibody (13-6800, Invitrogen), goat polyclonal anti-Lipocalin-2/

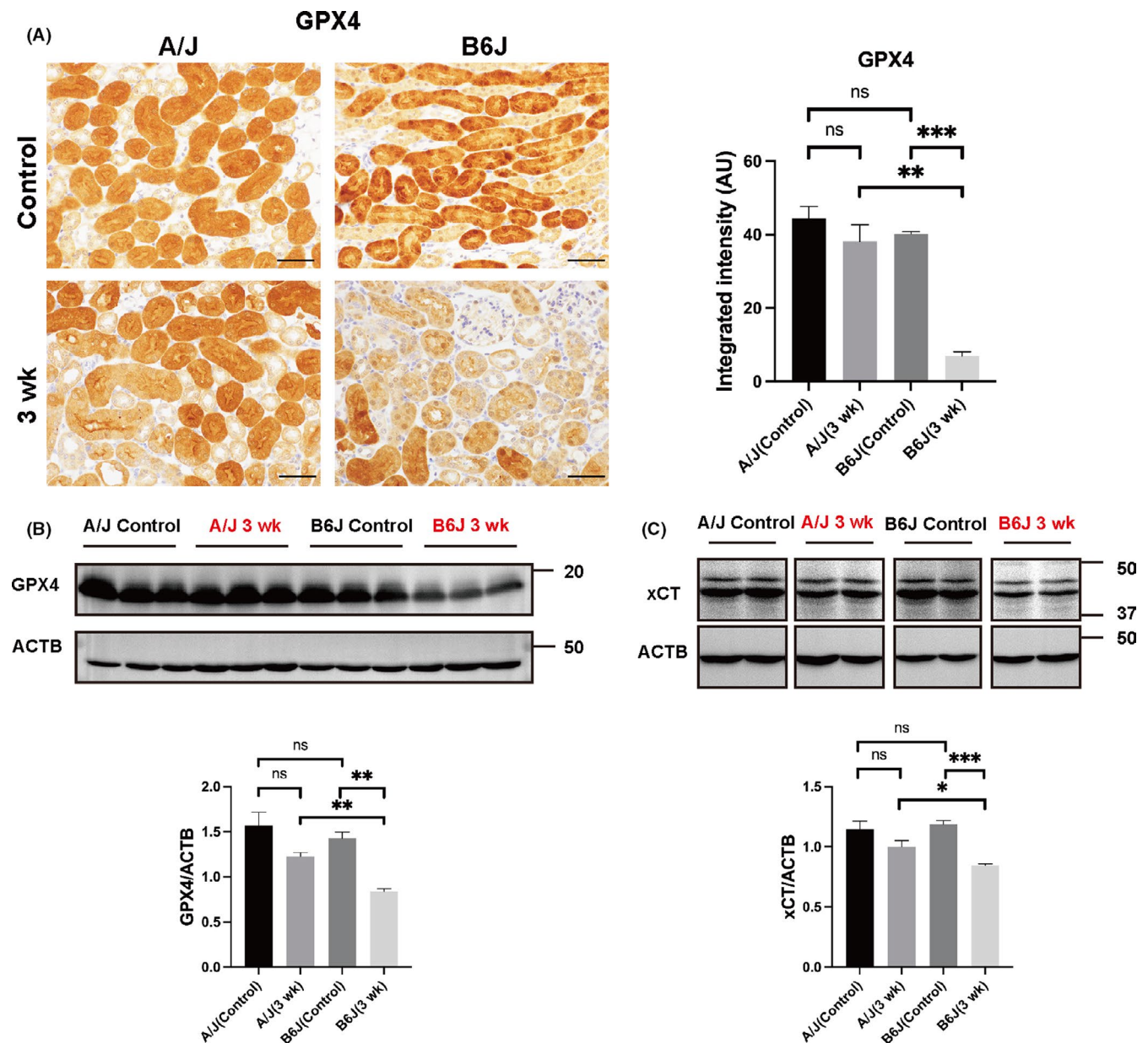


**FIGURE 3** High expression of glutathione peroxidase 4 (GPX4) in A/J mice after repeated intraperitoneal (i.p.) administration of ferric nitrilotriacetate (Fe-NTA) for 3 weeks. (A) Immunohistochemistry (IHC) analysis of GPX4 (bar = 50  $\mu$ m; N = 3). (B) Immunoblot analysis of GPX4 (N = 3). (C) Immunoblot analysis of cystine-glutamate antiporter (xCT) (N = 3; mean  $\pm$  SEM; \* $P$  < .05, \*\* $P$  < .01, \*\*\* $P$  < .001; ns, not significant)

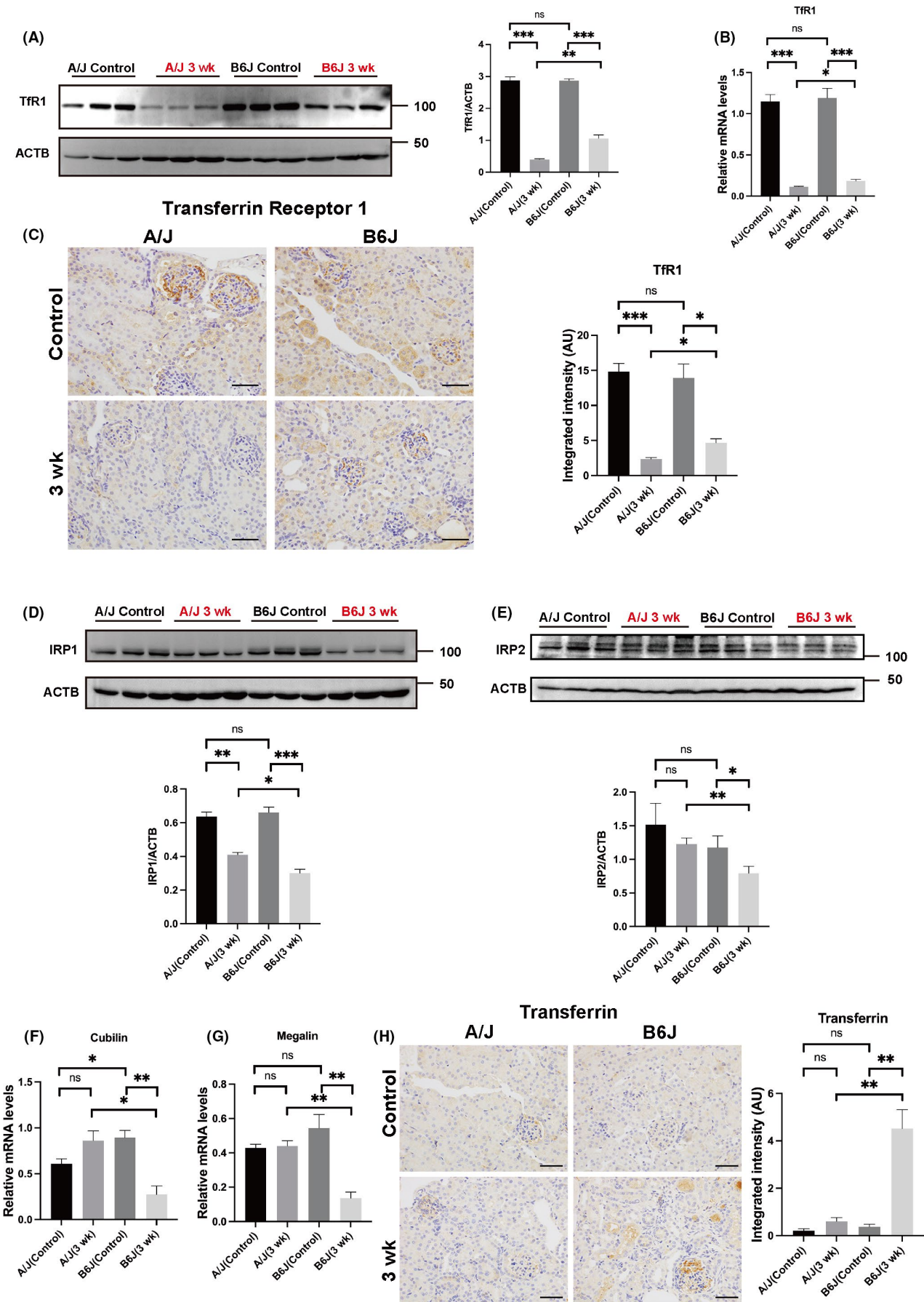


**FIGURE 4** Difference in responses of iron regulatory/metabolism proteins between *A/J* and *C57BL/6J* mice to repeated intraperitoneal (i.p.) administration of ferric nitrilotriacetate (Fe-NTA) for 3 weeks. (A) Immunoblot analysis of Transferrin receptor 1 (TfR1) (N = 3). (B) Real-time quantitative PCR (qPCR) analysis of *TfR1* (N = 5 for control; N = 4 for *A/J*; N = 3 for *C57BL/6J*). (C) Immunohistochemistry (IHC) analysis of TfR1 (bar = 50  $\mu$ m). (D, E) Immunoblot analysis of IRP1 and IRP2 (lower band; N = 3). (F, G) Real-time qPCR analysis of *Cubilin* and *Megalin* (N = 3). (H) IHC analysis of Transferrin in renal proximal tubular cells (bar = 50  $\mu$ m; N = 3; mean  $\pm$  SEM; \**P* < .05, \*\**P* < .01, \*\*\**P* < .001; ns, not significant). Refer to text for details

NGAL antibody (AF1857, R&D systems), rabbit monoclonal anti- $\beta$ -actin (ACTB) antibody (AC026, Abclonal), rabbit monoclonal anti-IRP1 antibody (ab126595, Abcam), rabbit polyclonal anti-IRP2 antibody (NB100-1798, Novus), rabbit polyclonal anti-FTH1 antibody (3998, CST), rabbit polyclonal anti-ferritin light chain (FTL) antibody (ab69090, Abcam), rabbit polyclonal anti-divalent metal transporter 1 (DMT1) antibody (20507-1-AP, proteintech), rabbit polyclonal anti-8-hydroxy-2'-deoxyguanosine (8-OHdG) antibody (bs1278R, Bioss), rabbit polyclonal anti-4-Hydroxynonenal antibody (bs6313R, Bioss), anti-CD10 antibody (ab256494, Abcam), anti-Ki67 antibody (ab16667, Abcam), rabbit monoclonal anti-Cleaved Caspase-3 antibody (9664, CST), rabbit monoclonal anti-Glutathione Peroxidase 4 antibody (ab125066, Abcam), and anti-xCT antibody (NB300-318, Novus). Secondary antibodies used in immunoblot analysis and immunohistochemistry were as follows: HRP-conjugated polyclonal Goat anti-Rabbit antibody (P0448, DAKO), HRP-conjugated polyclonal Rabbit anti-mouse antibody (P0260, DAKO) and HRP-conjugated polyclonal Rabbit anti-Goat antibody (P0160, DAKO).

## 2.6 | Real-time quantitative PCR

Total RNA from kidneys was extracted using the RNeasy Plus Mini Kit (74136, QIAGEN), which was quantified by the NanoDrop2000 (Thermo Fisher Scientific) and reverse-transcribed into cDNA using SuperScript III First-Strand (Invitrogen). The quantitative PCR (qPCR) was performed using Platinum SYBR Green (Invitrogen) on the CFX96 Real-Time System (Bio-Rad). The gene expression was calculated using the  $2^{-\Delta\Delta Ct}$  method and compared to the control group. The following primers were used for amplification in RT-qPCR: *TfR1*-F: 5'-TCCGCTCGTGGAGACTACTT-3', *TfR1*-R: 5'-ACATAGGGCGACAGGAAGTG-3', *Lcn2*-F: 5'-TGGAAGAACC AAGGAGCTGT-3', *Lcn2*-R: 5'-CACACTCACCACCCATTCAG-3', *Cubilin*-F: 5'-GAAGGGGATTCTCTGGAG-3', *Cubilin*-R: 5'-ACAG GGGTGTCTCCTGTAC-3', *Megalin*-F: 5'-TGTCTCTGCTGGGGTC TTCT-3', *Megalin*-R: 5'-GGGTGCCATCATTGGTAATC-3', and  $\beta$ -actin-F: 5'-TGTTACCAACTGGGACGACA-3',  $\beta$ -actin-R: 5'-GGGG TGTTGAAGGTCTCAAAA-3'.

## 2.7 | Detection of catalytic Fe(II)

RhoNox-4 (FerroOrange) was obtained from Goryo Kayaku. Kidneys of *A/J* and *C57BL/6J* mice were dissected 6 hours after a single Fe-NTA i.p. injection (5 mg iron/kg). The kidney tissues were embedded in plastic cryomold filled with Optimal Cutting Temperature compound (Sakura Finite Japan) immediately after excision, using dry ice

acetone. Frozen sections were cut using cryostat (Leica, CM1520). Then, the detection was performed as described<sup>25</sup> by applying Rhonox-4 on the frozen kidney sections, which were observed with a fluorescence microscope (BZ-9000, Keyence). The intensity of fluorescence was evaluated by ImageJ.

## 2.8 | Array-based comparative genomic hybridization analysis of ferric nitrilotriacetate-induced renal cell carcinoma

We extracted genomic DNA from RCC samples using a DNeasy Blood and Tissue Kit (QIAGEN), which was quantified by NanoDrop2000 (Thermo Fisher Scientific). Concentration of dsDNA was measured with a Quant-iT dsDNA BR Assay Kit (Thermo Fisher Scientific). We labeled DNA from 8 *A/J* mice RCC cases with Cy-5 and the corresponding control DNA with Cy-3, which were applied to the mouse genome CGH microarray slides 4x180k (G4826A, Agilent Technologies) according to the Agilent Oligonucleotide Array-Based CGH for Genomic DNA Analysis Protocol Ver.7.3. The data from the Agilent scanner was analyzed using the Agilent Genomic Workbench Standard Edition.

## 2.9 | Statistical analysis

All the statistical analyses were performed using GraphPad Prism 9. The significance of difference was calculated by unpaired *t* test and log-rank (Mantel-Cox) test. Significance was defined either as \**P* < .05, \*\**P* < .01, or \*\*\**P* < .001 or not significant (ns).

## 3 | RESULTS

### 3.1 | Incidence of ferric nitrilotriacetate-induced renal cell carcinoma is significantly higher in *A/J* mice than in *C57BL/6J* mice

The incidence of Fe-NTA-induced RCC in *A/J* mice (62.1%) was significantly higher than that of *C57BL/6J* mice in our recent study (7.1%).<sup>13</sup> After repeated i.p. Fe-NTA administration for 12 weeks, the long-term survival rate in *A/J* mice was consistently lower than that in *C57BL/6J* mice (Figure 1A). Mice that died during the 12-week Fe-NTA treatment period were excluded from the count. Other than RCC, 2 cases of lung adenocarcinoma and 6 cases of malignant lymphoma were also observed in *A/J* and *C57BL/6J* mice, respectively (Table 1). A significantly higher incidence of RCC was observed in *A/J* mice (Figure 1B). We observed macroscopic tumors in all cases, with

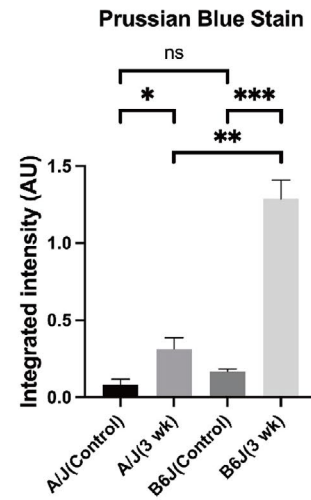
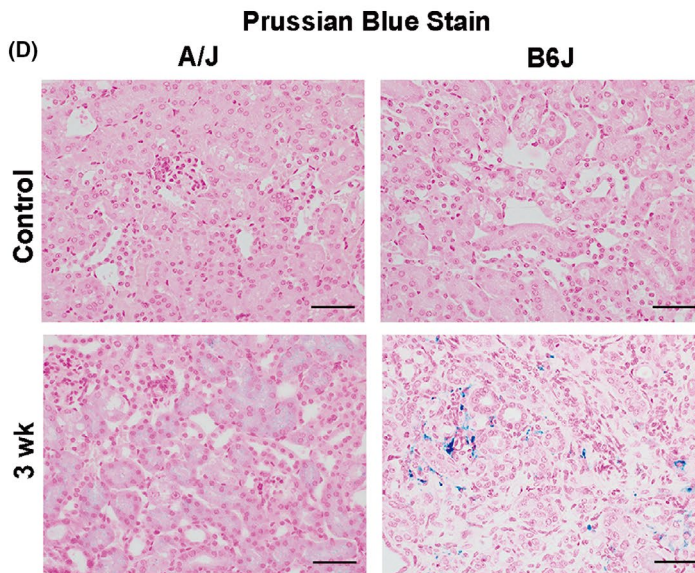
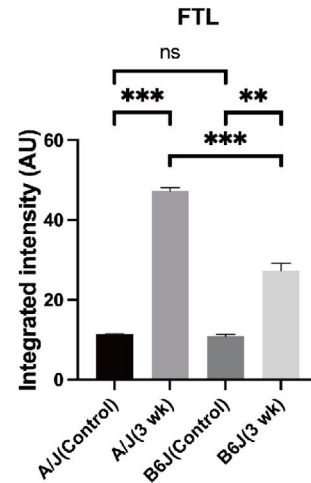
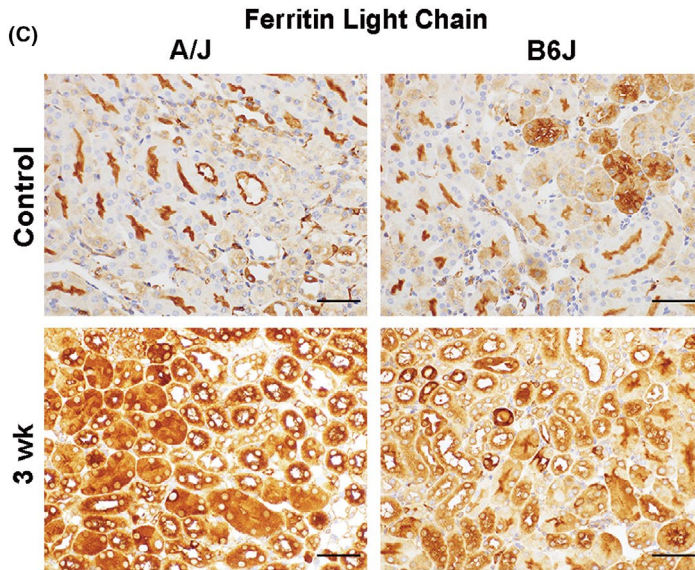
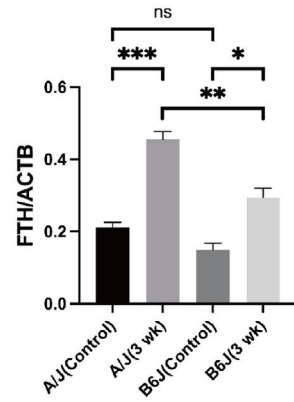
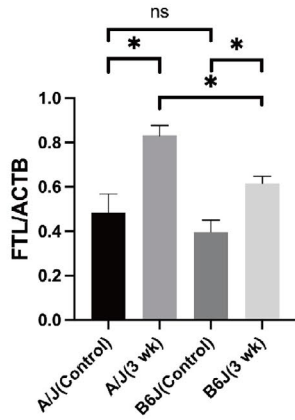
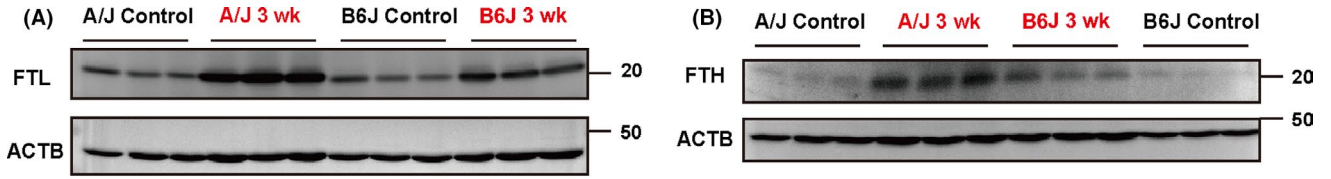




**FIGURE 5** Difference in levels of ferritin and hemosiderin between *A/J* and *C57BL/6J* mice after repeated intraperitoneal (i.p.) administration of ferric nitrilotriacetate (Fe-NTA) for 3 weeks. (A, B) Immunoblot analysis of ferritin light chain (FTL) and ferritin heavy chain (FTH) ( $N = 3$ ). (C) Immunohistochemistry (IHC) analysis of FTL (bar = 50  $\mu\text{m}$ ;  $N = 3$ ). (D) Prussian blue staining (bar = 50  $\mu\text{m}$ ;  $N = 3$ , mean  $\pm$  SEM; \* $P < .05$ , \*\* $P < .01$ , \*\*\* $P < .001$ ; ns, not significant)

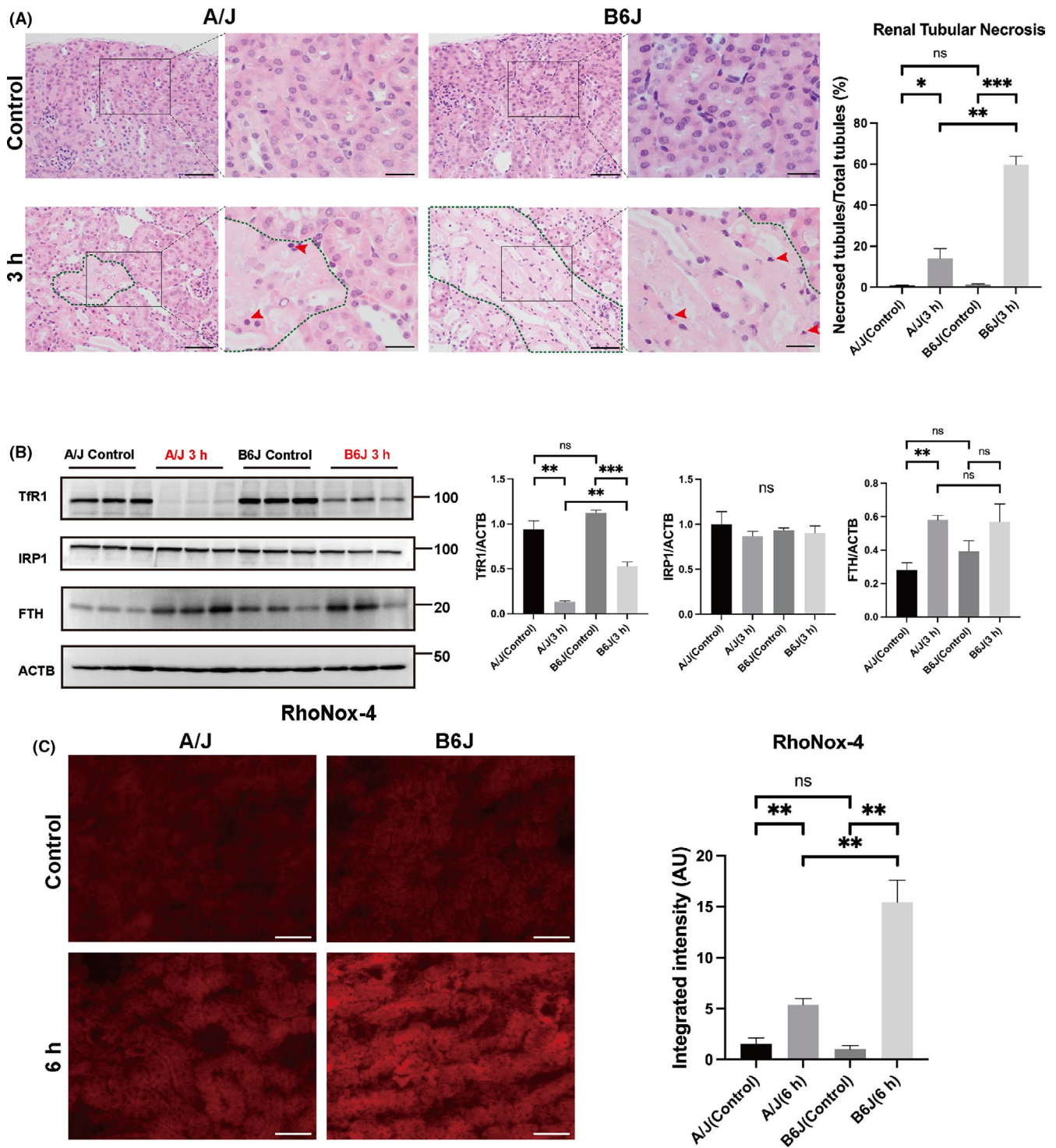


**FIGURE 6** Ferroptosis resistance in the acute phase of *A/J* mice by difference of renal tubular necrosis, iron regulatory/metabolism proteins and catalytic Fe(II) after single intraperitoneal (i.p.) administration of ferric nitrilotriacetate (Fe-NTA). (A) Histological analysis of renal proximal tubular damage at 3 h. Green dotted lines delineate the region of renal tubular necrosis. Red arrow heads, pyknosis (bar = 50  $\mu\text{m}$  or 20  $\mu\text{m}$  in each right magnified panel;  $N = 3$ ). (B) Immunoblot analysis of Transferrin receptor 1 (TfR1), IRP1, and ferritin heavy chain (FTH) at 3 h ( $N = 3$ ). (C) RhoNox-4 fluorescent staining for catalytic Fe(II) of proximal tubular cells (bar = 50  $\mu\text{m}$ ;  $N = 3$ , mean  $\pm$  SEM; \* $P < .05$ , \*\* $P < .01$ , \*\*\* $P < .001$ ; ns, not significant)

some tumors that were huge cysts. Proliferation of atypical glandular cells with CD10 immunopositivity was observed, presenting as either papillary, irregularly tubular, or solid structures with loss of normal renal tubular organization (Figures 1C and S1). Ki-67 immunostaining showed increased positivity in *A/J* RCC (Figure 1D). Table S1 describes further details of these RCC.

We performed the array-based CGH analysis on Fe-NTA-induced *A/J* mice RCC from the 8 cases, revealing  $\geq 5$  mm in diameter RCC (GEO accession: GSE183173). We found wide chromosomal deletions in chromosome 4 in all the cases and in chromosome 12, 13 or 14 in some cases (Figures 1E and S2). No homozygous loss of a tumor suppressor gene was detected in *C57BL/6J* mice RCC in the previous study,<sup>13</sup> whereas *Cdkn2a/2b* has been recognized as one of the target genes in iron-induced carcinogenesis.<sup>26</sup> In this study, we first found *Cdkn2a/2b* homozygous loss in 1 case and hemizygous loss in 3 RCC cases of *A/J* mice. *Tp73* (*p73*), a member of the *p53* family of tumor suppressor genes,<sup>27</sup> was hemizygously deleted in 7 out of 8 RCC examined. Distinct from Fe-NTA-induced rat RCC,<sup>16</sup> amplification of *Met* was not observed in *A/J* mice RCC. We also listed other genes reported to be associated with hereditary kidney cancer syndromes,<sup>28</sup> such as *PTEN*, *FLCN*, and *VHL*, which revealed no significant alterations (Figure 1F).

### 3.2 | Ferroptosis is repressed in *A/J* mice with decreased lipid peroxidation after subacute renal injury

GPX4 directly regulates membrane-associated lipid peroxidation<sup>29</sup> and is considered a key regulator of ferroptosis.<sup>30</sup> Histologically, we observed significantly less damage in renal tubular cells of *A/J* mice than *C57BL/6J* mice 3 weeks after repeated administration of Fe-NTA (Figure 2A). To evaluate the level of lipid peroxidation, we examined the levels of 4-hydroxy-2-nonenal (4-HNE)-modified proteins via immunohistochemistry. We found that 4-HNE was highly abundant in the nucleus of proximal tubular cells of *C57BL/6J* mice but not in *A/J* mice (Figure 2B). High Ki-67 positivity suggests simultaneous regenerative changes in *C57BL/6J* mice (Figure 2C).

Lipid peroxidation can be quenched by GPX4,<sup>31</sup> a well-known negative regulator of ferroptosis.<sup>32</sup> Persistently high expression of GPX4 in *A/J* mice was observed with immunohistochemistry (Figure 3A). Immunoblotting showed that *A/J* mice but not *C57BL/6J* mice can sustain high expression of GPX4 after 3-week Fe-NTA treatment (Figure 3B). Cystine-glutamate antiporter (*xCT*), encoded by *Slc7A11*, is an important regulator of GPX4.<sup>32</sup> The high expression of *xCT* was observed in *A/J* mice after 3-week Fe-NTA treatment but not in *C57BL/6J* mice (Figure 3C).

### 3.3 | Transferrin receptor is downregulated in *A/J* mice after subacute renal injury

To further study the responsible molecular mechanism for susceptibility to renal carcinogenesis, we explored the alteration of iron metabolism-associated genes. TfR1 is a major receptor for iron-loaded transferrin, regulating cellular iron intake.<sup>3</sup> TfR1 expression decreased in both strains after 3-week Fe-NTA administration, with significantly lower expression in *A/J* mice than in *C57BL/6J* mice (Figure 4A). This was confirmed both by mRNA measurement (Figure 4B) and immunohistochemistry (Figure 4C).

Kidneys play an essential role in preventing iron loss and monitoring iron status in the whole body. Iron metabolism in kidneys is mainly regulated by the iron response element-iron regulatory protein (IRE-IRP) system.<sup>33</sup> We measured the expression levels of IRP1 and IRP2 in *A/J* and *C57BL/6J* mice after 3-week Fe-NTA treatment via immunoblotting. Notably, we observed higher retained expression of IRP1 and IRP2 in *A/J* mice than in *C57BL/6J* mice (Figure 4D,E). Megalin-cubilin receptor complex is also an important iron transporter in the kidney that is highly correlated with TfR1 expression.<sup>2,34</sup> mRNA levels of *megalyn* and *cubilin* were significantly downregulated in *C57BL/6J* mice in the 3-week group (Figure 4F,G). High expression of transferrin was observed in *C57BL/6J* mice in the 3-week group (Figure 4H). We observed no difference in the expression of DMT1 between the two strains (Figure S3A).

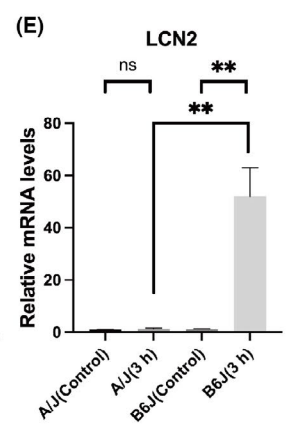
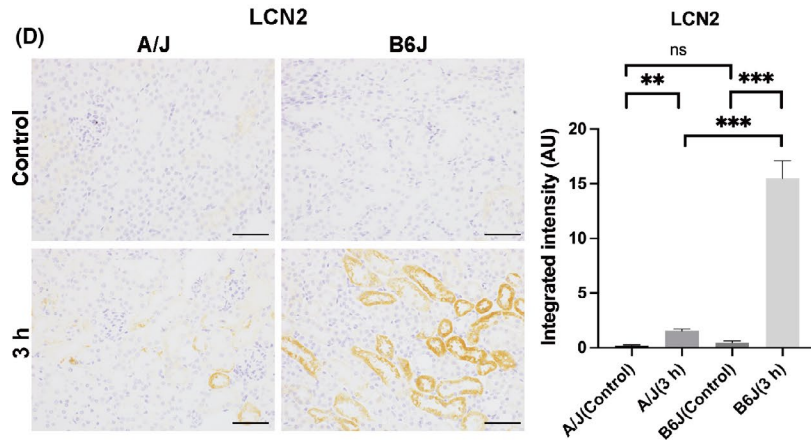
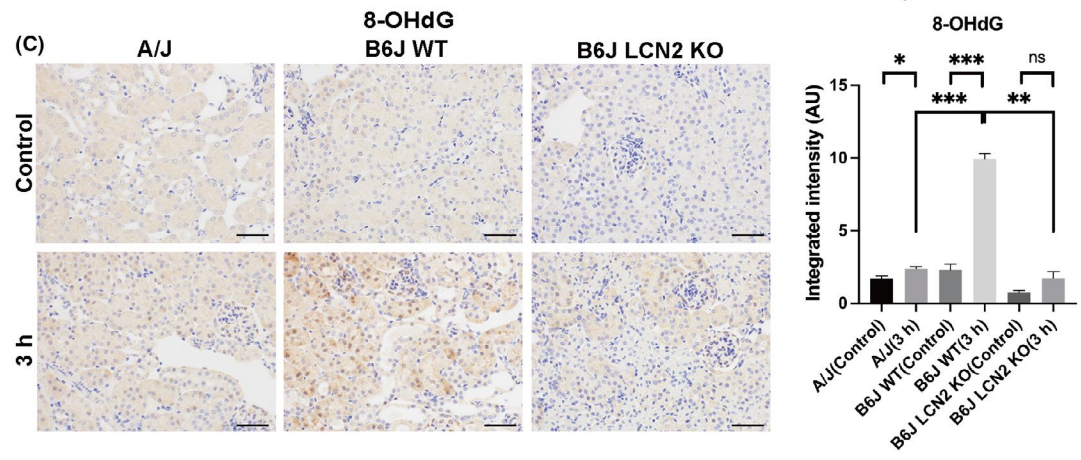
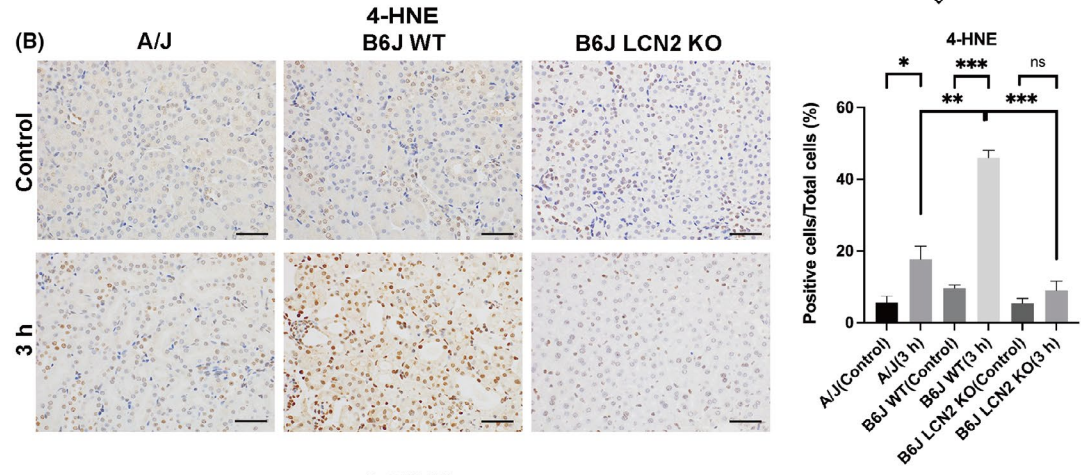
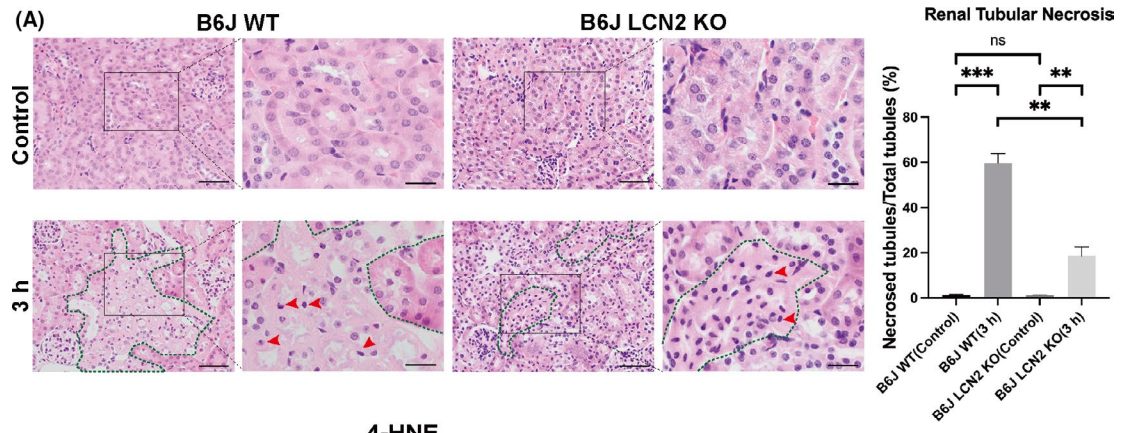
### 3.4 | Higher induction of ferritin in *A/J* mice after subacute renal injury

Ferritin can store superfluous cellular iron as insoluble Fe(III) in protein cores, detoxifying catalytic Fe(II)<sup>35</sup> to prevent unnecessary Fenton reaction.<sup>36</sup> Both FTL and ferritin heavy chain (FTH) were more significantly increased after subacute renal injury in *A/J* mice than in *C57BL/6J* mice (Figure 5A,B), which was consistent with immunohistochemical analysis (Figure 5C). Iron staining with Prussian blue was more prominent in *C57BL/6J* mice than in *A/J* mice, especially in the stroma area (Figure 5D).

### 3.5 | Both ferroptosis and apoptosis are suppressed in *A/J* mice during acute renal injury

We then studied the relationship between iron metabolism and cell death 3 hours after single Fe-NTA injection. Renal proximal tubules of *C57BL/6J* mice presented more damage than was the case in *A/J*

**FIGURE 7** LCN2 is proportionally associated with renal tubular ferroptosis induced by ferric nitrilotriacetate (Fe-NTA) in the acute phase. (A) Histological analysis of renal proximal tubular damage in *C57BL/6J* wild-type and *Lcn2* (*-/-*) mice. Green dotted lines delineate the region of renal tubular necrosis. Red arrow heads, pyknosis (bar = 50  $\mu$ m or 20  $\mu$ m in each right magnified panel; N = 3). (B) Immunohistochemistry (IHC) analysis of 4-hydroxy-2-nonenal (4-HNE) (bar = 50  $\mu$ m, N = 3). (C) IHC analysis of 8-hydroxy-2'-deoxyguanosine (8-OHdG) (bar = 50  $\mu$ m, N = 3). (D) IHC analysis of LCN2 (bar = 50  $\mu$ m, N = 3 for control and N = 4 for 3-h group). (E) Real-time quantitative PCR (qPCR) analysis of *Lcn2* (N = 4, mean  $\pm$  SEM; \**P* < .05, \*\**P* < .01, \*\*\**P* < .001; ns, not significant)



mice. Abundant tubular necrosis with nuclear pyknosis as ferroptosis was observed in *C57BL/6J* mice (Figure 6A). TfR1 expression was more significantly decreased in *A/J* mice, whereas there was no difference in IRP1 and FTH expression (Figure 6B). We previously reported the increase in catalytic Fe(II) with RhoNox-1 in the same acute phase of Fe-NTA-induced renal tubular injury in rats.<sup>25</sup> Here we used RhoNox-4, a more sensitive probe, and found that catalytic Fe(II) is significantly higher in *C57BL/6J* mice than in *A/J* mice 6 hours after Fe-NTA administration, confirming that cell death mode includes ferroptosis (Figure 6C).

LCN2, a siderophore-binding protein, is a sensitive biomarker for acute renal tubular injury in humans and an iron transporter in kidneys.<sup>23,37</sup> Acute renal tubular injury was significantly reversed in *C57BL/6J Lcn2 (-/-)* mice (Figure 7A), which was confirmed with 4-HNE and 8-OHdG immunostaining (Figure 7B,C). Immunohistochemical staining of LCN2 in proximal tubules 3 hours after Fe-NTA administration in *C57BL/6J* mice was more prominent than in *A/J* mice (Figure 7D). mRNA levels of *Lcn2* in *C57BL/6J* were 50-fold higher than in *A/J* mice, indicating higher acute tubular injury (Figure 7E). However, the GPX4 level was not altered (Figure S3B).

Cleaved caspase-3, a marker of apoptosis, was significantly increased in *C57BL/6J wild-type* mice but not in *A/J wild-type* mice and *C57BL/6J LCN2 (-/-)* mice in the 3-h group (Figure S4A,B). Nuclear fragmentations were confirmed only in *C57BL/6J wild-type* mice (Figure S4C). We observed high expression of LCN2 in *C57BL/6J* mice from the 3-week group (Figure S4D). However, cleaved caspase-3 was not increased in the 3-week group (Figure S4E).

## 4 | DISCUSSION

The Fe-NTA-induced renal carcinogenesis model is distinctive in that *wild-type* rats acquire somatic mutations frequently found in human cancers, such as *Cdkn2a/2b* homozygous deletion.<sup>38,39</sup> Notably, the association of excess iron as carcinogenic milieu and *Cdkn2a/2b* homozygous deletion is well known.<sup>9,16</sup> This deletion-type mutation permanently provides cells with apoptosis inhibition and removes cell-cycle brakes. In this study, we have established a difference in cancer susceptibility for murine strains: the incidence of Fe-NTA-induced RCC is markedly higher in *A/J* mice than in *C57BL/6J* mice. This was associated with an additional mechanism, ferroptosis resistance. We also included the *C3H/HeJ* mouse strain for the carcinogenesis experiment, in which 36 male mice out of 50 died during the 3-month Fe-NTA administration period, and 2 mice developed RCC out of 14 mice (data not shown). With array-based CGH, we observed *Cdkn2a/2b* homozygous loss for the first time in a murine RCC of *A/J* strain mouse. We believe that this small fraction is associated with the species difference between mice and rats/humans. Mouse genome may require higher integrity than rats/humans for cell survival, or mouse cells may allow permanent proliferation with less stringent genomic/expressional alterations than in rats and humans.<sup>40</sup> Deletion of *Cdkn2a* inhibits cyclin-dependent kinases to

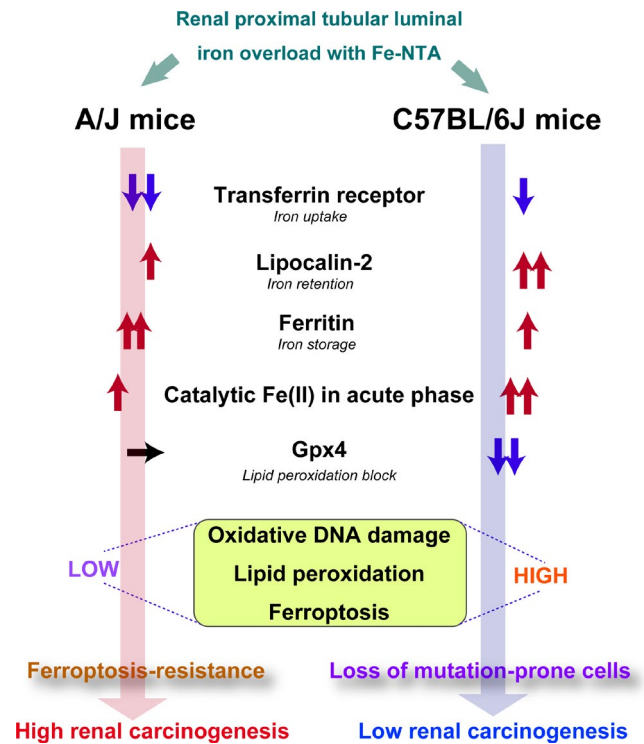


FIGURE 8 A schema of difference in ferric nitrilotriacetate (Fe-NTA)-induced renal carcinogenesis between *A/J* and *C57BL/6J* mice

promote DNA replication,<sup>26</sup> and *TP73* and *Arf* downregulation can repress the apoptosis.<sup>27</sup>

We hypothesized that cancer susceptibility might be associated with ferroptosis,<sup>31,41,42</sup> a catalytic Fe(II)-dependent regulated necrosis<sup>43</sup> accompanying lipid peroxidation, in which a major product is 4-HNE.<sup>44</sup> A lipid repair enzyme GPX4<sup>45</sup> was more highly expressed in *A/J* mice than in *C57BL/6J* mice in the 3-week group. xCT (SLC7A11), cystine/glutamate antiporter, by providing GPX4 with its substrate glutathione, can provide major resistance to ferroptosis.<sup>20</sup> Our results indicate that ferroptosis resistance by counteracting oxidative stress was inherently observed in *A/J* strain mice.

Transferrin receptor 1 expression was decreased in the subacute renal injury experiments, with the decrease being more significant in the *A/J* strain. Cellular iron metabolism, including TfR1, is under the control of the IRE/IRP system,<sup>46</sup> a post-transcriptional regulation.<sup>47</sup> We observed a contradictory result that there was still a higher expression of IRP1/IPR2 in *A/J* mice with a low level of *TfR1* mRNA, which may suggest that the total amount or the compartmental fraction of iron may be different between *A/J* and *C57BL/6J* strains. Contrary to *TfR1*, mRNA levels of *cubilin* and *megalyn* were higher in *A/J* mice than in *C57BL/6J* mice. Megalin and cubilin are multiligand endocytic receptors that can absorb transferrin iron by endocytosis in kidney proximal tubule epithelial cells.<sup>48</sup> Reciprocal regulation of TfR1 and cubilin-megalin complex has been reported in proximal tubules.<sup>2</sup> After releasing iron, holo-transferrin will be apo-transferrin, which is recycled and redistributed on plasma membrane.<sup>49</sup> Intriguingly, when the cubilin and megalin become the main iron receptor, apo-transferrin will be directly sent to lysosomes for

degradation, instead of being recycled, to repress the iron import,<sup>48</sup> which is consistent in our results in *A/J* mice. *A/J* mice may have a more efficient mechanism to control iron import to prevent excess iron-mediated renal tubular damage.

Increased ferritin can store insoluble Fe(III) by oxidizing catalytic Fe(II) to protect the host from excess iron,<sup>50</sup> thus preserving iron safely in ferritin.<sup>35</sup> Further, Prussian blue staining, detecting mainly insoluble Fe(III) in lysosomes, including hemosiderin,<sup>51</sup> is increased in *C57BL/6J* mice, indicating a higher level of iron overload in *C57BL/6J* mice than in *A/J* mice. Thus, high expression of ferritin under less iron overload is another ferroptosis resistance mechanism in *A/J* mice.

An acute 3-h study provided us with similar results. More severe renal tubular damage and relatively high expression of TfR1 were observed in *C57BL/6J* mice in the 3-h group. Reportedly, LCN2 increases intracellular iron accumulation and promotes the cellular level of ROS via mammalian siderophores.<sup>23,52</sup> To measure catalytic Fe(II) levels in proximal tubular cells, we used a sensitive turn-on fluorescent probe RhoNox-4. We observed a lower level of catalytic Fe(II) in *A/J* mice expressing lower levels of LCN2 and TfR1 in comparison to *C57BL/6J* mice. We confirmed that higher LCN2 expression was correlated with oxidative stress. In *Lcn2* ( $-/-$ ) mice, the damage of renal tubules and high lipid peroxidation was reversed, indicating that LCN2 deficiency can alleviate Fe-NTA-induced oxidative renal tubular injury. LCN2 is captured by megalin and degraded in proximal tubular cells but not recycled.<sup>34,53</sup> Our results in *A/J* mice are consistent with this reciprocal association between LCN2 and megalin. Taken together, low levels of TfR1 and LCN2 contribute to ferroptosis resistance in *A/J* mice.

LCN2 induces apoptosis in cardiomyocytes with iron accumulation.<sup>52</sup> Caspase-3, as a marker of apoptosis,<sup>54</sup> was highly expressed in *C57BL/6J* wild-type mice 3 hours after Fe-NTA injection but not in *A/J* wild-type mice and *C57BL/6J Lcn2* ( $-/-$ ) mice. We assume that oxidative stress by catalytic Fe(II) increased DNA damage and triggered the cascades of apoptosis in *C57BL/6J* mice.<sup>55,56</sup> Of note, this caspase activation was not observed in the 3-week group, suggesting that apoptosis is a minor acute event.

The present study has some limitations. *C57BL/6J* are more sensitive to i.p. Fe-NTA injections, as described. The carcinogenesis experiments were designed under a concept of maximal tolerated exposure, resulting in different protocols for the two strains (*C57BL/6J*, 3-5 mg iron/kg of Fe-NTA for 12 weeks; *A/J* at the present study, 5-7 mg iron/kg of Fe-NTA for 12 weeks).

In conclusion, ferroptosis resistance is a key factor to determine susceptibility to iron-induced renal carcinogenesis. After Fe-NTA exposure, *A/J* mice can maintain an appropriate level of oxidative stress to induce oxidative DNA damage without excessive ferroptosis at an early stage, eventually leading to a high incidence of RCC (Figure 8). In this sense, *A/J* mice are a better model for genetic research of iron-induced renal carcinogenesis than *C57BL/6J* mice. Further studies are warranted on the application of the present murine data for human cancer prevention, where carcinogenic exposure is much longer but presumably lighter. We also have to consider the possibility that cancer resistance may

have a trade-off effect on other pathologies, such as infection susceptibility.

## ACKNOWLEDGMENTS

The authors thank Prof. Shizuo Akira (Immunology Frontier Research Center, Osaka University) for providing *Lcn2* ( $-/-$ ) mice. This work was supported, in part, by JST CREST (Grant Number JPMJCR19H4), JSPS Kakenhi (Grant Number JP19H05462 and JP20H05502), and a Research Grant from the Princess Takamatsu Cancer Research Fund (19-251). We thank Nobuaki Misawa (Department of Pathology and Biological Responses, Nagoya University Graduate School of Medicine) for excellent technical assistance.

## DISCLOSURE

The authors have no conflicts of interest to declare.

## ORCID

Takashi Takahashi  <https://orcid.org/0000-0003-0615-7001>

Shinya Toyokuni  <https://orcid.org/0000-0002-5757-1109>

## REFERENCES

1. Toyokuni S. Iron and thiols as two major players in carcinogenesis: friends or foes? *Front Pharmacol*. 2014;5:5-8.
2. van Swelm RPL, Wetzels JFM, Swinkels DW. The multifaceted role of iron in renal health and disease. *Nat Rev Nephrol*. 2020;16:77-98.
3. Kawabata H. Transferrin and transferrin receptors update. *Free Radic Biol Med*. 2019;133:46-54.
4. Yanatori I, Kishi F. DMT1 and iron transport. *Free Radic Biol Med*. 2019;133:55-63.
5. Sponkel HT, Alfrey AC, Hammond WS, et al. Effect of iron on renal tubular epithelial cells. *Kidney Int*. 1996;50:436-444.
6. Ebina Y, Okada S, Hamazaki S, et al. Nephrotoxicity and renal cell carcinoma after use of iron- and aluminum-nitilotriacetate complexes in rats. *J Natl Cancer Inst*. 1986;76:107-113.
7. Martinez AMF, Masereeuw R, Tjalsma H, et al. Iron metabolism in the pathogenesis of iron-induced kidney injury. *Nat Rev Nephrol*. 2013;9:385-398.
8. Capitanio U, Montorsi F. Renal cancer. *Lancet*. 2016;387:894-906.
9. Toyokuni S, Ito F, Yamashita K, Okazaki Y, Akatsuka S. Iron and thiol redox signaling in cancer: an exquisite balance to escape ferroptosis. *Free Radic Biol Med*. 2017;108:610-626.
10. Okada S, Minamiyama Y, Hamazaki S, Toyokuni S, Sotomatsu A. Glutathione cycle dependency of ferric nitilotriacetate-induced lipid peroxidation in mouse proximal renal tubules. *Arch Biochem Biophys*. 1993;301:138-142.
11. Okada S. Iron-induced tissue damage and cancer: the role of reactive oxygen species-free radicals. *Pathol Int*. 1996;46:311-332.
12. Li JL, Okada S, Hamazaki S, Ebina Y, Midorikawa O. Subacute nephrotoxicity and induction of renal cell carcinoma in mice treated with ferric nitilotriacetate. *Cancer Res*. 1987;47:1867-1869.
13. Li GH, Akatsuka S, Chew SH, et al. Fenton reaction-induced renal carcinogenesis in *Mutyh*-deficient mice exhibits less chromosomal aberrations than the rat model. *Pathol Int*. 2017;67:564-574.
14. Toyokuni S. Iron-induced carcinogenesis: The role of redox regulation. *Free Radic Biol Med*. 1996;20:553-566.
15. Toyokuni S. The origin and future of oxidative stress pathology: from the recognition of carcinogenesis as an iron addiction with ferroptosis-resistance to non-thermal plasma therapy. *Pathol Int*. 2016;66:245-259.

16. Akatsuka S, Yamashita Y, Ohara H, et al. Fenton reaction induced cancer in wild type rats recapitulates genomic alterations observed in human cancer. *PLoS One*. 2012;7:1-10.
17. Kakhlon O, Cabantchik ZI. The labile iron pool: characterization, measurement, and participation in cellular processes. *Free Radic Biol Med*. 2002;33:1037-1046.
18. Kehrer JP. The Haber-Weiss reaction and mechanisms of toxicity. *Toxicology*. 2000;149:43-50.
19. Dixon SJ, Lemberg KM, Lamprecht MR, et al. Ferroptosis: an iron-dependent form of nonapoptotic cell death. *Cell*. 2012;149:1060-1072.
20. Cao JY, Dixon SJ. Mechanisms of ferroptosis. *Cell Mol Life Sci*. 2016;73:2195-2209.
21. Cheng Y, Zak O, Aisen P, Harrison SC, Walz T. Structure of the human transferrin receptor-transferrin complex. *Cell*. 2004;116:565-576.
22. Feng H, Schorpp K, Jin J, et al. Transferrin receptor is a specific ferroptosis marker. *Cell Rep*. 2020;30:3411-3423.e7.
23. Xiao X, Yeoh BS, Vijay-Kumar M. Lipocalin 2: an emerging player in iron homeostasis and inflammation. *Annu Rev Nutr*. 2017;37:103-130.
24. Flo TH, Smith KD, Sato S, et al. Lipocalin 2 mediates an innate immune response to bacterial infection by sequestering iron. *Nature*. 2004;432:917-921.
25. Mukaide T, Hattori Y, Misawa N, et al. Histological detection of catalytic ferrous iron with the selective turn-on fluorescent probe RhoNox-1 in a Fenton reaction-based rat renal carcinogenesis model. *Free Radic Res*. 2014;48:990-995.
26. Toyokuni S. Mysterious link between iron overload and CDKN2A/2B. *J Clin Biochem Nutr*. 2011;48:46-49.
27. Maas AM, Bretz AC, Mack E, Stiewe T. Targeting p73 in cancer. *Cancer Lett*. 2013;332:229-236.
28. Shuch B, Zhang J. Genetic predisposition to renal cell carcinoma: Implications for counseling, testing, screening, and management. *J Clin Oncol*. 2018;36:3560-3566.
29. Gaschler MM, Stockwell BR. Lipid peroxidation in cell death. *Biochem Biophys Res Commun*. 2017;482:419-425.
30. Yang WS, Stockwell BR. Ferroptosis: death by lipid peroxidation. *Trends Cell Biol*. 2016;26:165-176.
31. Toyokuni S, Yanatori I, Kong Y, et al. Ferroptosis at the crossroads of infection, aging and cancer. *Cancer Sci*. 2020;111:2665-2671.
32. Dixon SJ, Stockwell BR. The hallmarks of ferroptosis. *Annu Rev Cancer Biol*. 2019;3:35-54.
33. Meyron-Holtz EG, Ghosh MC, Iwai K, et al. Genetic ablations of iron regulatory proteins 1 and 2 reveal why iron regulatory protein 2 dominates iron homeostasis. *EMBO J*. 2004;23:386-395.
34. Smith CP, Lee WK, Haley M, et al. Proximal tubule transferrin uptake is modulated by cellular iron and mediated by apical membrane megalin-cubilin complex and transferrin receptor 1. *J Biol Chem*. 2019;294:7025-7036.
35. Nakamura T, Naguro I, Ichijo H. Iron homeostasis and iron-regulated ROS in cell death, senescence and human diseases. *Biochim Biophys Acta - Gen Subj*. 2019;1863:1398-1409.
36. Swaminathan S. Iron homeostasis pathways as therapeutic targets in acute kidney injury. *Nephron*. 2018;140:156-159.
37. Chakraborty S, Kaur S, Guha S, Batra SK. The multifaceted roles of neutrophil gelatinase associated lipocalin (NGAL) in inflammation and cancer. *Biochim Biophys Acta - Rev Cancer*. 2012;1826:129-169.
38. Tanaka T, Iwasa Y, Kondo S, Hiai H, Toyokuni S. High incidence of allelic loss on chromosome 5 and inactivation of *p15(INK4B)* and *p16(INK4A)* tumor suppressor genes in oxystress-induced renal cell carcinoma of rats. *Oncogene*. 1999;18:3793-3797.
39. Hiroyasu M, Ozeki M, Kohda H, et al. Specific allelic loss of *p16<sup>INK4A</sup>* tumor suppressor gene after weeks of iron-mediated oxidative damage during rat renal carcinogenesis. *Am J Pathol*. 2002;160:419-424.
40. Akatsuka S, Li GH, Toyokuni S. Superiority of rat over murine model for studies on the evolution of cancer genome. *Free Radic Res*. 2018;52:1323-1327.
41. Yan H-F, Zou T, Tuo Q-Z, et al. Ferroptosis: mechanisms and links with diseases. *Signal Transduct Target Ther*. 2021;6(1):49.
42. Hassannia B, Vandenabeele P, Vanden Berghe T. Targeting Ferroptosis to iron out cancer. *Cancer Cell*. 2019;35:830-849.
43. Koppenol WH, Hider RH. Iron and redox cycling. Do's and don'ts. *Free Radic Biol Med*. 2019;133:3-10.
44. Breitzig M, Bhimineni C, Lockey R, Kolliputi N. 4-Hydroxy-2-nonenal: a critical target in oxidative stress? *Am J Physiol - Cell Physiol*. 2016;311:C537-C543.
45. Yang W, SriRamaratnam R, Welsch M, et al. Regulation of ferroptotic cancer cell death by GPX4. *Cell*. 2014;156:317-331.
46. Wilkinson N, Pantopoulos K. The IRP/IRE system in vivo: insights from mouse models. *Front Pharmacol*. 2014;5:1-15.
47. Gammella E, Buratti P, Cairo G, Recalcati S. The transferrin receptor: the cellular iron gate. *Metallomics*. 2017;9:1367-1375.
48. Christensen EI, Birn H. Megalin and cubilin: Multifunctional endocytic receptors. *Nat Rev Mol Cell Biol*. 2002;3:258-268.
49. Wang J, Pantopoulos K. Regulation of cellular iron metabolism. *Biochem J*. 2011;434:365-381.
50. Anderson CP, Shen M, Eisenstein RS, Leibold EA. Mammalian iron metabolism and its control by iron regulatory proteins. *Biochim Biophys Acta - Mol Cell Res*. 2012;1823:1468-1483.
51. Taguchi S, Hidaka S, Yanai M, et al. Renal hemosiderosis presenting with acute kidney injury and macroscopic hematuria in Immunoglobulin A nephropathy: a case report. *BMC Nephrol*. 2021;22:1-6.
52. Xu G, Ahn JH, Chang SY, et al. Lipocalin-2 induces cardiomyocyte apoptosis by increasing intracellular iron accumulation. *J Biol Chem*. 2012;287:4808-4817.
53. Mori K, Lee HT, Rapoport D, et al. Endocytic delivery of lipocalin-siderophore-iron complex rescues the kidney from ischemia-reperfusion injury. *J Clin Invest*. 2005;115:610-621.
54. Pawar RD, Pitashny M, Gindea S, et al. Neutrophil gelatinase-associated lipocalin is instrumental in the pathogenesis of antibody-mediated nephritis in mice. *Arthritis Rheum*. 2012;64:1620-1631.
55. Zhou BO, Zhang J-Y, Liu X-S, et al. Tom20 senses iron-activated ROS signaling to promote melanoma cell pyroptosis. *Cell Res*. 2018;28:1171-1185.
56. Alarifi S, Ali D, Alkahtani S, Alhader MS. Iron oxide nanoparticles induce oxidative stress, DNA damage, and caspase activation in the human breast cancer cell line. *Biol Trace Elem Res*. 2014;159:416-424.

## SUPPORTING INFORMATION

Additional supporting information may be found in the online version of the article at the publisher's website.

**How to cite this article:** Cheng Z, Akatsuka S, Li GH, Mori K, Takahashi T, Toyokuni S. Ferroptosis resistance determines high susceptibility of murine A/J strain to iron-induced renal carcinogenesis. *Cancer Sci*. 2021;00:1-14. <https://doi.org/10.1111/cas.15175>